ACS OMEGA

Open Access

http://pubs.acs.org/journal/acsodf

Article

Constructing a Microdiffusion−Seepage−Stress Multifield Coupling Model for Nanopore Gas

Pingdingqi Tuo, Haifeng Wang,* Lu Cunyang, and Zhang Xinghua

Cite This: *ACS Omega* 2024, 9, 28207−28217

Read Online

ACCESS | Metrics & More | Article Recommendations

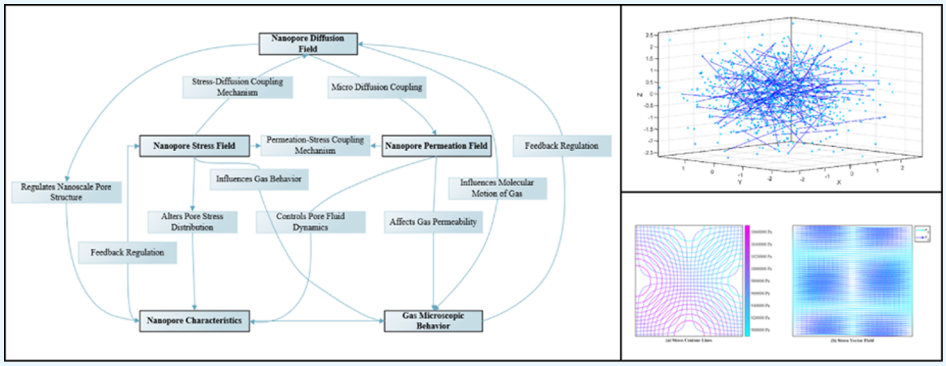

ABSTRACT: Existing research is difficult to fully capture the correlation between gas molecules and pore wall interactions, multiphase flow, and stress distribution in nanopores. Taking gas as an example, a microscopic model was constructed. At the same time, diffusion, seepage, and stress were considered to accurately predict and manage gas transport in nanopores. First, molecular dynamics (MD) simulation methods were adopted to simulate the motion trajectories and interactions of gas molecules in nanopores. Second, a multiscale model was established based on continuum mechanics to consider the interaction between pore walls and gas molecules, and a diffusion equation was established to describe the diffusion process of gas molecules in pores. Then, finite element analysis and porous media models were used to simulate the seepage behavior of gas in the nanopores. Finally, the stress distribution in the pores was analyzed, and the influence of the interaction between the pore wall and gas molecules on stress was considered. The multifield coupling model was experimentally evaluated from three aspects: diffusion coefficient, seepage behavior, and stress distribution. The root-mean-square error (RMSE) and mean absolute error (MAE) of the model in different testing directions were calculated using different simulation tools, such as COMSOL, ANSYS, OpenFOAM, and CFX. The mean values of RMSE and MAE were lower than 0.20 and 0.17, respectively. The constructed model can comprehensively describe gas transmission within nanopores, improving the management accuracy and efficiency.

1. INTRODUCTION

Nanopores are a common occurrence in nature and engineering fields, and the diffusion and seepage behavior of gas molecules within them are crucial for gas transmission in fields such as mines, oil fields, and gas storage. However, the complex correlation between the interaction of gas molecules and the pore wall,[1,2] multiphase flow,[3,4] and stress distribution in nanopores[5,6] makes it difficult for existing studies to fully capture these processes.[7,8] Currently, an integrated multifield coupling model is needed to accurately predict and manage gas transport in nanopores.

In previous studies, many scholars have devoted their studies to exploring the mechanisms of gas transport in nanopores. Their research focuses mainly on diffusion and seepage phenomena, but these two processes are usually separated and studied independently.[9,10] Regarding the candidate material for gas separation membranes—nanoporous graphene, scholars such as Yuan[11] developed transport kinetics related to direct impact of graphene body and surface diffusion of graphene adsorption layer. In exploring the gas diffusion behavior under nano constraints, Yin,[12] and others proposed the local effective diffusivity lattice Boltzmann model (LED-LBM). Combining the Fick's first law to study the transport characteristics of CH_4 and C_2H_6 in shale potassium Illite nanopores, scholars such as Zhang[13] estimated the thermodynamic factor, self-diffusion coefficient, Maxwell−Stefan (MS),

Received: February 18, 2024
Revised: May 5, 2024
Accepted: May 9, 2024
Published: June 19, 2024

and transport diffusion coefficient of $CH_4-C_2H_6$. To solve the deficiency of Darcy's law in characterizing gas mobility in shale reservoirs, Hu[14] and other scholars built an apparent permeability (AP) model for shale reservoirs. Considering the effect on gas−water flow and the simulation of hydraulic fracturing fractures, Huang[15] developed a numerical model applicable to the entire Nussen range of shale gas reservoirs. He deeply analyzed the effect of different flow regimes on the dynamic permeability of shale. In the field of nonlinear seepage research in tight reservoirs, scholars such as Wu[16] proposed an analytical nanofluid dynamics model to describe the flow characteristics of pressurized oil in nanoscale pores with a diameter greater than 2 nm. Although current research methods can effectively describe the mechanism of gas transport, there are shortcomings in considering interactions and stress distribution,[17,18] leading to a lack of comprehensive and profound understanding of the details and complexity of gas transport in nanopores. This issue also highlights the potential improvement space in the field of nanopore gas transport research.

Some researchers have attempted to use multifield coupling models to comprehensively describe the interrelationships between diffusion, seepage, and stress in response to the problem of gas transport within nanopores. Usually, methods such as MD simulation,[19,20] computational fluid dynamics,[21,22] and lattice Boltzmann[23,24] are used for research. To uncover the multiscale flow mechanism of methane in coal, Li[25] and other scholars established a permeability model considering tandem multiscale pores to reflect the effects of flow regime, stress, and pore pressure. Based on Langmuir's theory, researchers such as Huang[26] established a synthesized AP model coupling the surface diffusion of adsorbed gases, sloshing flow taking into account the additional fluxes generated by surface diffusion and Knudsen diffusion. For the transport process of methane in carbon nanopores, Zhang[27] and others simulated the arrangement, slip, and transition flow of wall atoms in the supercritical state and the application of different driving forces on the basis of MD theory. Facing the problem that the characteristic parameters of coal diffusion under stress conditions are hard to obtain, Tian[28] and other scholars used a multifield coupling model to calculate the methane transport in the coal body in the process of borehole extraction under different stresses. In order to conduct experiments on the diffusion behavior of shale gas under high temperature and pressure conditions, Sun[29] proposed a new approach for calculating the multifield coupling diffusion coefficient by using molecular membrane samples with uniform pore sizes instead of shale cores. Taking into account stress sensitivity, real gas effect, and adsorption mechanisms, Zhang[30] successfully created a new apparent permeability model by adjusting parameters and conducting model sensitivity analysis. Considering the combined effects of moisture content and constraint effects on gas phase critical properties, Sun[31] and others developed a fully coupled analytical model and found that the confinement effect significantly increased the apparent gas permeability when the pore radius was less than 5 nm. When the pore radius was within the range of 1−2 nm, the gas effect increased by an average of 4.38%. However, existing methods have some limitations in the process of building models, such as high computational costs[32,33] and difficulty, in applying them to practical engineering problems.[34,35] A new method was adopted to comprehensively address the MD behavior, percolation phenomenon, and stress distribution of gas molecules in nanopores, thereby more accurately solving the problem of gas transport in nanopores.

A comprehensive microscopic model was constructed in the study, taking into account diffusion, seepage, and stress to accurately predict and manage gas transport behavior in nanopores. The relative displacement between molecules was calculated, and the potential function was used to calculate attraction and repulsion. For the interaction between molecules and pore walls, the potential barrier and attraction on the pore wall and the motion of molecules on the pore wall were considered. The interaction between gas molecules and pore walls in nanopores was considered through continuous medium mechanics modeling. The surface of nanopores was defined as a pore wall, and a parametrized equation of the surface was used to represent the geometric shape of the pore wall. The continuum mechanics equation was used to depict the macroscopic flow behavior of gas in nanopores, and the results of microscopic MD simulations were input as boundary conditions into the macroscopic continuum mechanics equation. By coupling methods, microsimulation and macrosimulation were connected to achieve the establishment of multiscale models. The diffusion equation was utilized to depict the diffusion behavior of gas molecules in the nanopores. Finally, the finite element method (FEM) was utilized to solve the equation, and the simulation region was divided into finite elements and numerically solved within each element. The stress changes caused by the interaction between pore wall stress and gas molecules were coupled to obtain the global stress distribution within the nanopores. In the experimental section, the constructed multifield coupling model was used to investigate the actual case of methane gas diffusion in underground gas storage, and experimental tools such as COMSOL, ANSYS, OpenFOAM, and CFX were used for testing and simulation. The results indicated that the model had mean RMSE values of 0.19, 0.19, 0.20, and 0.20 for different testing directions and mean MAE values of 0.14, 0.17, 0.16, and 0.15, respectively. The model can accurately describe the gas transmission within nanopores. The innovation of the research lies in the construction of a microdiffusion−seepage−stress multifield coupling model for nanopore gas, which helps to improve the accuracy and efficiency of gas transmission management in fields such as mines, oil fields, and gas storage.

2. MD SIMULATION

The main structural parameters of the gas are described in Table 1.

Table 1 shows the structural parameters of the main gas molecules in gas, and a gas molecular model is constructed using these parameters. The molecular models of N_2, CH_4, and CO_2 are shown in Figure 1. Among the five main molecules, N_2, CH_4, and CO_2 were chosen as the focus of the study due to their representativeness and importance in fields such as gas

Table 1. Gas Structure Parameters

gas molecule	bond length (Å)	bond angle (deg)
hydrogen (H_2)	0.74	104.5
nitrogen (N_2)	1.10	180
oxygen (O_2)	1.21	180
methane (CH_4)	C−H: 1.09	H−C−H: 109.5
carbon dioxide (CO_2)	C−O: 1.16	C−O−C: 180

https://doi.org/10.1021/acsomega.4c01572
ACS Omega 2024, 9, 28207−28217

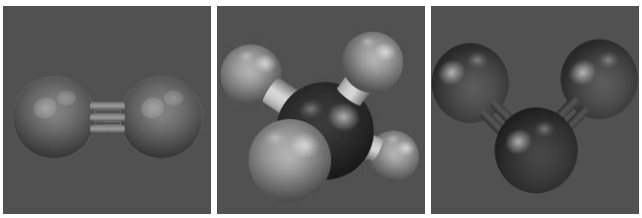

Figure 1. N_2, CH_4, and CO_2 molecular models.

transport and energy storage. They exhibit different diffusion and percolation behaviors with significant variations in their behavior within nanopores, providing rich information for understanding gas transport in nanopores.

The constructed N_2, CH_4, and CO_2 molecular models are shown in Figure 1. To explore the motion trajectories and interactions of gas molecules in nanopores, the study simulates the motion and interactions of gas molecules in nanopores to study the macroscopic properties of substances.

First, a simulation system is constructed. Model nanopores with different pore sizes and shapes are selected, and gas molecules are introduced into them, constructed as eq 1

$$\Omega = \{r_i, v_i\} \tag{1}$$

Here, Ω represents the entire simulation system, including positions r_i and velocities v_i of all of the molecules. The Lennard−Jones potential function is utilized to represent the interaction between gas molecules, as shown in eq 2

$$U(r_{ij}) = 4\epsilon\left[\left(\frac{\sigma}{r_{ij}}\right)^{12} - \left(\frac{\sigma}{r_{ij}}\right)^{6}\right] \tag{2}$$

Among them, $U(r_{ij})$ represents the potential energy between molecular pairs, ϵ and σ are the parameters of the potential function, and r_{ij} is the distance between molecular pairs. In MD simulation, Newton's second law is utilized to depict the motion of gas molecules while solving the evolution of the position and velocity of each molecule over time. The equation of motion is shown in eq 3

$$m_i\frac{d^2r_i}{dt^2} = F_i \tag{3}$$

Here, m_i is the mass of the i-th molecule, r_i is its position vector, and F_i is the force acting on the molecule. To solve the equation, the forces acting on each molecule are calculated.

To calculate the interaction force, the previously defined potential function is used. For interactions between molecules, their relative displacements are calculated, and potential functions are used to calculate attraction and repulsion. The calculation of the interaction force is shown in eq 4

$$F_i = -\nabla U(r_i) \tag{4}$$

Among them, $\nabla U(r_i)$ represents the gradient of potential function U on the position vector. The visualization of the process of simulating molecular motion is shown in Figure 2.

Figure 2 shows the simulation of the motion trajectories and interactions of gas molecules in the nanopores. The light blue circles are used to represent molecules, and the dark blue lines are used to represent interactions between molecules. X, Y, and Z axes together constitute the relative positions of gas molecules in space. The simulation of gas molecules' motion

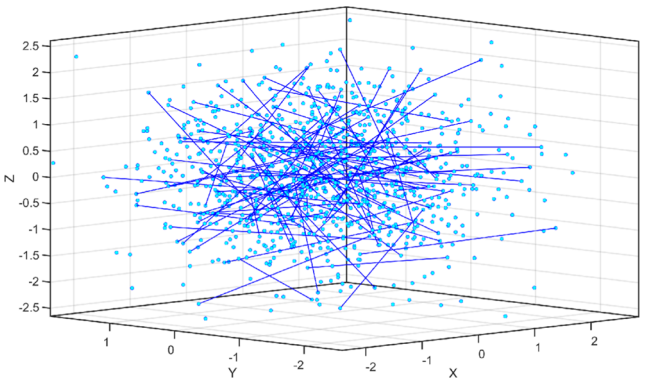

Figure 2. Simulated molecular motion process.

trajectories and interactions in nanopores using GROMACS software is configured as follows: simulation system size: length 50 nm, width 50 nm, height 50 nm; gas molecule type: methane (CH_4). Total number of molecules: about 10,000; initial temperature: 300 K; pressure: 1 atm; time step: 1 fs; total simulation time: 100 ns; Lennard−Jones potential parameters: ϵ = 0.210 kJ/mol, σ = 3.8 Å; boundary conditions: periodic; and data collection frequency: every 1 ps. To solve the equations of motion, numerical integration methods are used to discretize the positions and velocities of molecules over time to simulate their motion. At the same time, appropriate time steps are selected to ensure the stability and accuracy of the simulation. The numerical integration form is shown in eq 5

$$r_i(t + \Delta t) = r_i(t) + v_i(t)\Delta t + \frac{F_i}{2m_i}(\Delta t)^2 \tag{5}$$

Among them, Δt is the time step. Continuum medium mechanics modeling is performed to consider the interaction between gas molecules and pore walls within the nanopores. The surface of nanopores is defined as a pore wall, and a parametrized equation of the surface is used to represent the geometric shape of the pore wall. The position vector function in the Cartesian coordinate system is shown in eq 6

$$r = (x, y, z) \tag{6}$$

Here, r represents the position vector of a point on the surface, and x, y, and z are the coordinate components similar to those in MD simulations. Equation 2 is used to represent the attraction and repulsion forces between gas molecules and pore walls. The continuum mechanics equation is utilized to depict the macroscopic flow behavior of gas in nanopores, and the Navier−Stokes equation is used to describe fluid flow, as shown in eqs 7 and 8

$$\frac{\partial\rho}{\partial t} + \nabla\cdot(\rho u) = 0 \tag{7}$$

$$\rho\left(\frac{\partial u}{\partial t} + (u\cdot\nabla)u\right) = -\nabla p + \nabla\cdot\tau \tag{8}$$

Among them, ρ is the gas density, u is the velocity field, t is the time, p is the pressure, ∇ is the gradient operator, and τ is the viscous stress tensor. The equation describes the conservation of mass and momentum of gas in the pores. Appropriate boundary conditions are defined to simulate flow within pores: wall conditions are represented by boundary conditions, including velocity and pressure on the wall; the adsorption

https://doi.org/10.1021/acsomega.4c01572
ACS Omega 2024, 9, 28207−28217

Table 2. Key Parameter Setting

parameter type	detailed description	value
wall velocity	the speed of fluid movement along the pore walls.	0.005 m/s
wall pressure	pressure exerted by the fluid on the pore walls, affecting stress distribution and seepage behavior within the pores.	1,050,000 Pa
pore size	diameter of the nanopores. The size of the pores directly affects the movement and distribution of gas molecules within.	50 nm
temperature	the temperature of the simulation environment, influencing the thermal motion and reaction kinetics of gas molecules. Higher temperatures increase molecular activity.	300 K
gas molecule diameter	diameter of the gas molecules used in the simulation. The size of the molecules significantly impacts intermolecular interactions and adsorption behavior.	0.3 nm
gas molecule interaction parameter	interaction strength between gas molecules considered in molecular dynamics simulation.	0.8 kJ/mol

conditions are represented by modifying the rebound and adsorption behavior of gas molecules on the pore wall. Table 2 lists the key parameters and explains their rationale.

The results of microscopic MD simulations are input as boundary conditions into macroscopic continuum mechanics equations. The study adopts a coupling method to connect microsimulation and macrosimulation, achieving the establishment of multiscale models. The coupling method can consider the interaction between gas molecules and pore walls at different scales, achieving comprehensive multifield coupling analysis.

3. ESTABLISHMENT OF DIFFUSION EQUATION

The diffusion equation is utilized to depict the diffusion behavior of gas molecules in nanopores, as shown in eq 9

$$\frac{\partial C}{\partial t} = D\nabla^2 C \tag{9}$$

Here, $\frac{\partial C}{\partial t}$ is the rate of change of concentration over time; D is the diffusion coefficient, expressed as a constant related to temperature and gas; and ∇^2 is the Laplace operator, representing the second-order spatial gradient of concentration. Considering the interaction between gas molecules and the pore wall, potential energy barrier U is introduced to represent the energy barrier that gas molecules need to overcome when crossing the pore wall. The potential energy barrier is obtained through MD simulation, and diffusion coefficient D is modified to consider the interaction, as shown in eq 10

$$D = D_0 \exp\left(-\frac{U}{k_B T}\right) \tag{10}$$

Among them, D_0 is the standard diffusion coefficient, which is related to the diffusion rate in the absence of an interaction. U is the potential energy barrier, k_B is the Boltzmann constant, and T is the temperature. As a key component of the diffusion equation solution, boundary conditions are used to describe the interaction between gas molecules in the pores and pore walls. In the nanopores, the following boundary conditions are used for the study.

At the surface of the pore wall, the normal component of diffusion flux J_s is zero, meaning that there is no mass passing through the pore wall surface. The Neumann boundary condition is represented in eq 11

$$n\cdot\nabla C = 0 \tag{11}$$

Here, n is the surface normal vector. The Langmuir-type adsorption model is utilized to represent the adsorption phenomenon of gas molecules on the pore wall surface, as shown in eq 12

$$J_s = k_a(C_{eq} - C) \tag{12}$$

Among them, k_a is the adsorption rate constant, and C_{eq} is the equilibrium concentration.

After the diffusion equation and boundary conditions are determined, the interaction simulation visualization of gas molecules in pores and pore walls is shown in Figure 3. To

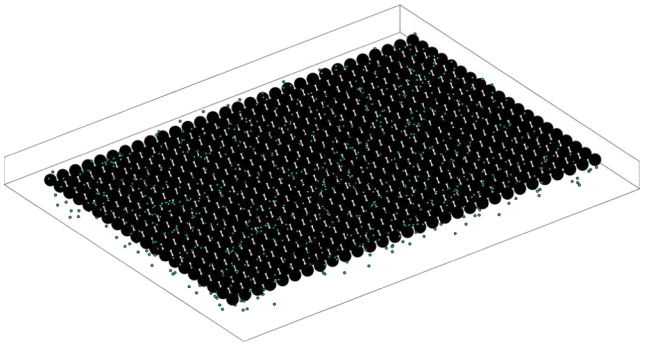

Figure 3. Interaction simulation of gas molecules with pore walls in pores.

simulate gas microdiffusion and seepage behaviors in nanopores, the molecular dynamics simulation software LAMMPS was used, enabling precise modeling of interactions at the molecular level. The simulation covered a range of 10−50 nm to observe molecular behavior within the pores, with the diameter of the molecular pores set between 1 and 5 nm. Finite difference is used to obtain numerical solutions to obtain the concentration distribution of gas molecules in nanopores, as shown in Figure 4.

Figure 4a−c show the concentration distribution of N_2, CH_4, and CO_2 gas molecules in nanopores over time, respectively. The horizontal axis indicates time (h), and the vertical axis indicates gas volume fraction (%). From the graph, it can be learned that the volume fractions of N_2 and CH_4 gradually increase with time (30 to 240 h), increasing from 80.86 and 3.03 to 83.39 and 3.48%, respectively. CO_2 shows a decreasing trend overall, decreasing from 0.303 to 0.132%. The increase in volume fractions of nitrogen and methane over time is attributed to their behavior within pores, related to adsorption, desorption, and diffusion processes in nanopores. Over time, these gases enter the pore system from the surrounding environment and distribute more evenly within the pores, leading to an increase in their volume fractions. Conversely, the decrease in carbon dioxide's volume fraction is due to its replacement by other gases and its tendency to be

https://doi.org/10.1021/acsomega.4c01572
ACS Omega 2024, 9, 28207−28217

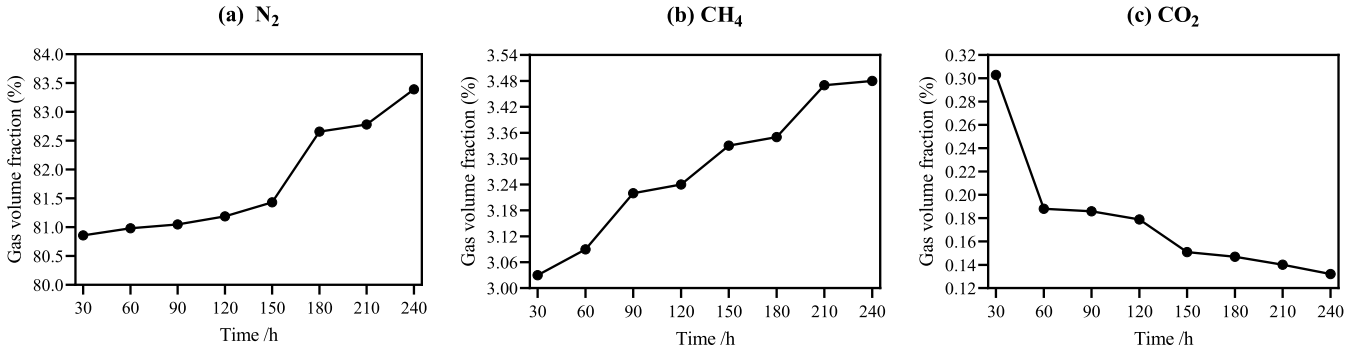

Figure 4. Concentration distribution of N_2, CH_4, and CO_2 gas molecules in nanopores over time. (a): N_2; (b): CH_4; and (c): CO_2.

more readily adsorbed on the pore surfaces due to interactions with pore walls.

The increase in the nitrogen and methane volume fractions over time in Figure 3 can be attributed to several factors rooted in physical principles. In nanoporous systems, gas molecules tend to exhibit diffusion behavior due to concentration gradients and are facilitated by interactions with the pore walls. As time progresses, gas molecules gradually diffuse through the nanopores, leading to accumulation within the pore space. Considering the Langmuir-type adsorption model introduced in eq 12, gas molecules tend to adsorb onto the pore walls. This adsorption phenomenon is driven by the affinity between gas molecules and the surface of the nanopores, which further contributes to the observed increase in volume fractions over time. Specifically, nitrogen and methane, as common components in natural gas reservoirs, exhibit a tendency to adsorb onto solid surfaces, including the pore walls studied in the nanoporous system. Therefore, the accumulation of nitrogen and methane within the nanopores increases over time due to the combined effects of the diffusion and adsorption processes.

4. DIFFUSION–SEEPAGE–STRESS MULTIFIELD COUPLING MODEL

During stress coupling, careful consideration was given to the influence of coal matrix expansion and deformation due to the gas pressure on the model. As the pressure increased from its initial state to a certain level, the volume of the coal matrix began to exhibit significant expansion, with the rate of expansion increasing with the pressure. The study also examined the effects of coal matrix expansion on the pore structure and permeability characteristics. Simulation analysis revealed that the expansion of the coal matrix led to changes in the pore structure, resulting in noticeable alterations in the pore size and distribution, thereby affecting gas permeation behavior. Under the influence of pressure, the expansion of the coal matrix caused changes in stress distribution, manifesting as enhanced nonuniformity in the stress field.

Ω is utilized to represent the entire simulation area. A subdomain containing nanopores is defined, and its geometric features can be described by parameter sets including pore diameter and shape. The porous medium model is used to depict the gas seepage in the nanopores. The basic assumptions of the model include the uniformity, permeability, and continuity of the pore medium, and the permeability is represented by permeability k. According to Darcy's law, seepage velocity q is directly proportional to permeability k and seepage pressure gradient ∇P, as shown in eq 13

$$q = -\frac{k}{\mu}\nabla P \tag{13}$$

Here, μ is the gas viscosity. The mathematical form of the seepage equation is shown in eq 14

$$\nabla \cdot q = -\nabla \cdot \left(\frac{k}{\mu}\nabla P\right) = 0 \tag{14}$$

This is an elliptical partial differential equation, where $\nabla\cdot$ represents the divergence operation. In the seepage simulation, the initial condition represents the seepage state at the beginning of the simulation, represented as the initial pressure field. Boundary conditions are used to describe the external constraints of the simulation area, represented as fixed pressure, fixed flow velocity, and no flow conditions. The FEM is used to address the equation, and the simulation area is divided into finite elements and numerically solved within each element. The discrete form of the seepage equation is shown in eq 15

$$\int_{\Omega} \nabla \cdot q \mathrm{d}\Omega = \int_{\Omega} 0 \mathrm{d}\Omega \tag{15}$$

After numerical solution, information about the gas seepage behavior in nanopores, including the seepage velocity, permeability, and pressure, is obtained, as shown in Table 3.

Table 3. Gas Seepage Velocity, Permeability, and Pressure under Nanopores

pore size (nm)	flow velocity (m/s)	permeability (m^2)	pressure (Pa)
5	0.003	0.8×10^{-8}	1,100,000
7	0.004	1.0×10^{-8}	1,050,000
8	0.004	1.0×10^{-8}	1,050,000
9	0.004	1.1×10^{-8}	1,020,000
10	0.005	1.2×10^{-8}	1,000,000
11	0.005	1.2×10^{-8}	980,000
12	0.006	1.8×10^{-8}	950,000
13	0.006	1.7×10^{-8}	940,000
14	0.007	1.6×10^{-8}	920,000
15	0.008	1.5×10^{-8}	900,000

Table 3 shows the gas seepage velocity, permeability, and pressure under different nanopore sizes. From the table, it can be learned that the larger the pore size (5 to 15 nm), the stronger the ability of the fluid to pass through, the higher the flow rate (0.003 to 0.008 m/s), and the lower the required pressure (1,100,000–900,000 Pa). The value of the permeability is related to the pore size and fluid properties. In the

https://doi.org/10.1021/acsomega.4c01572
ACS Omega 2024, 9, 28207–28217

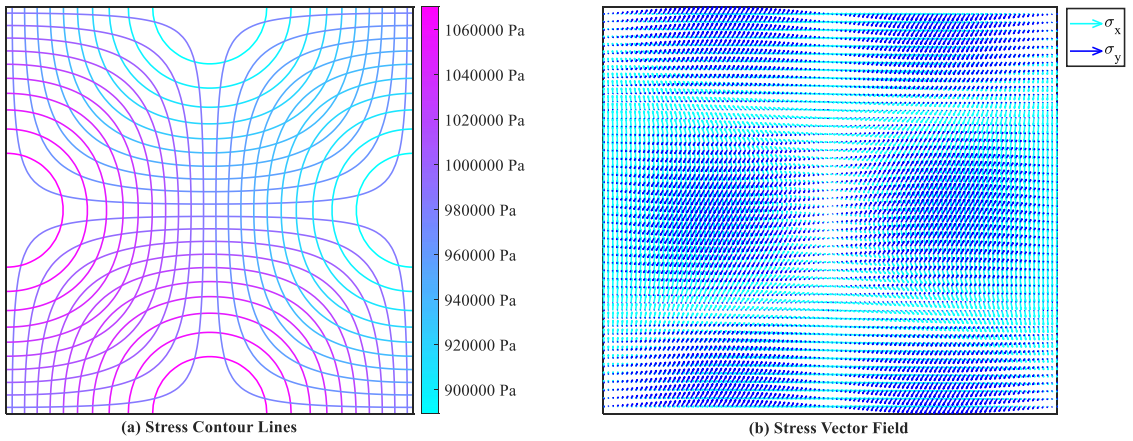

Figure 5. Global stress distribution within nanopores. (a): Stress contour line and (b): stress vector field.

smaller range of pore size, as the pore size increases, the permeability gradually increases (0.8×10^{-8}–1.8×10^{-8}); when the pore size increases to a certain extent, the permeability gradually decreases (1.8×10^{-8}–1.5×10^{-8}) due to changes in the flow characteristics of the fluid. When the pore size increases to a certain extent, the changing flow characteristics of the fluid lead to a gradual decrease in the permeability. In smaller pores, fluid flow is more laminar or streamlined, allowing for efficient passage through the pores. However, as the pore size increases, the flow becomes more turbulent, reducing the efficiency of fluid transport. This turbulence creates additional resistance and disrupts the direct passage of fluids, resulting in a decreased permeability.

According to the data in Table 3, the gradual decrease in permeability can be attributed to the fluid flow behavior within nanoscale pores. The phenomenon can be understood from the perspective of pore-scale fluid dynamics. Initially, as the pore size decreases, the fluid exhibits higher mobility due to enhanced pore accessibility and reduced tortuosity. Consequently, the permeability increases proportionally with increasing pore size within the observed range. With a continued increase in pore size, a critical threshold is reached, leading to a transition in fluid flow behavior. At larger pore sizes, the importance of viscous forces decreases relative to inertial forces, resulting in a transition from viscous-dominated to inertial-dominated flow regimes. In practice, this transition signifies a change in the mechanisms governing the fluid flow within the pores. Inertial-dominated flow mechanisms are characterized by increased flow resistance due to nonlinear interactions between the fluid and pore walls, leading to a decrease in permeability despite the larger pore size. Additionally, changes in fluid properties, such as viscosity and density, also influence flow behavior, further contributing to the observed decrease in permeability. The observed gradual decrease in permeability with increasing pore size in the nanoscale range is a consequence of the complex interplay between pore geometry, fluid properties, and the viscous and inertial flow mechanisms.

The basic equation of elasticity is used to describe the stress field, and the stress tensor is represented by Hook's Law, as shown in eq 16

$$\sigma = C \cdot \varepsilon \tag{16}$$

Here, σ is the stress tensor, C is the elastic tensor, and ε is the strain tensor. At the same time, the stress distribution on the surface of the hole wall is concerned, as calculated by eq 17

$$\sigma_2 = F/A \tag{17}$$

Among them, σ_2 shows the stress, F shows the force on the hole wall, and A shows the cross-sectional area of the hole wall. The influence of the interaction between gas molecules in pores on the stress distribution is considered. Among them, van der Waals force is a key factor, expressed in eq 18

$$F_{LJ} = -\nabla U_{LJ}(r) \tag{18}$$

Here, F_{LJ} represents the van der Waals force, ∇ represents the gradient operation, and U_{LJ} is the Lennard–Jones potential function mentioned earlier. Finally, the stress changes caused by the interaction between pore wall stress and gas molecules are coupled together to obtain global stress distribution within the nanopores. The stress contour and stress vector fields are shown in Figure 5.

Figure 5 shows the global stress distribution of gas within the nanopores. Among them, Figure 5a shows the stress contour line, showing the stress distribution map from 900,000 to 1,060,000 Pa, and the color bar shows the mapping between stress values and colors. Through the density and distribution of contour lines, it is possible to clearly see the changes in stress in the area and where the stress values are high/low. Figure 5b shows the stress vector field, showing the stress components along the X and Y axes, respectively. By analyzing the length and direction of each arrow, it is possible to clearly understand the magnitude and direction of stress and obtain information about the stress situation and possible stress flow at different points. Figure 5 shows the global stress distribution within nanopores, revealing the patterns of stress variation, especially the distribution of high- and low-stress areas in the nanopores. These findings are significant for future research, providing crucial insights into the behavior of stress in gas transmission within nanopores.

From Figure 5, it can be observed that the distribution of stress within the nanoscale pores is nonuniform. The density of the contour lines reflects the regions of stress concentration, with denser contour lines indicating higher stress gradients in those areas. These stress concentration regions are attributed to the irregularity of the pore wall geometry or the accumulation of gas molecules in specific regions. The color variation of the contour lines from blue to red represents a transition from low-stress to high-stress values. The stress vector field illustrates the stress components along the X and Y axes, where the length and direction of the arrows indicate the

https://doi.org/10.1021/acsomega.4c01572
ACS Omega 2024, 9, 28207−28217

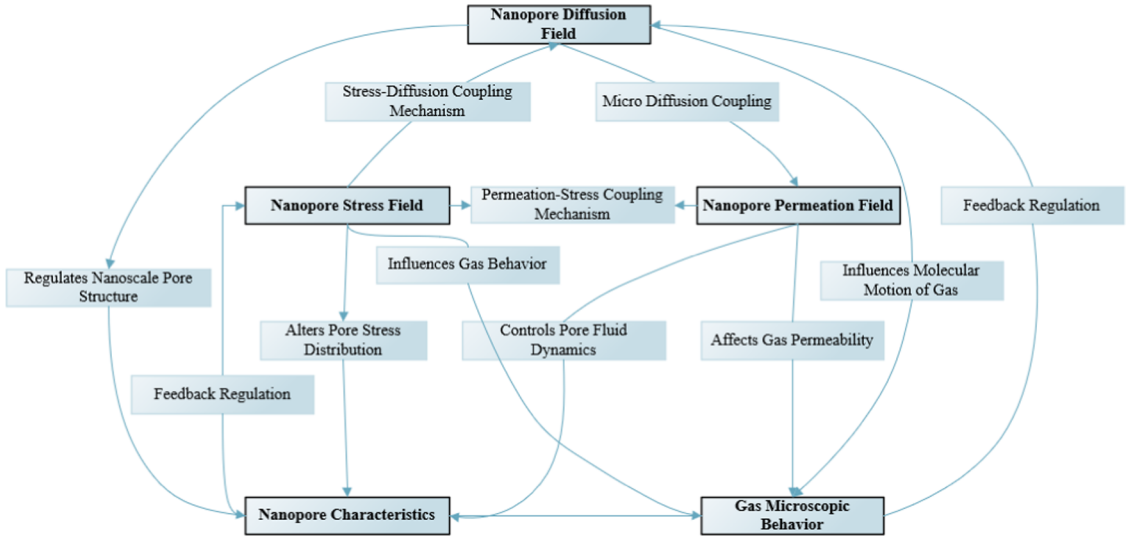

Figure 6. Diffusion−seepage−stress coupling relationship.

magnitude and direction of stress, respectively. Through these vectors, the mechanical interactions and intensities of gas molecules within the pore space can be qualitatively analyzed, providing deeper insights into the stress transfer mechanisms within nanoscale pores. In nanoscale pores, the movement and interaction of gas molecules result in variations in stress values across different regions. These variations manifest as differences in the contour line density in the stress contour plot and as arrows of varying lengths and directions in the stress vector field. This information regarding stress distribution is crucial for understanding the flow behavior in porous media, assessing reservoir mechanical stability, and optimizing extraction strategies. In unconventional gas extraction operations, it can help predict and mitigate gas anomalies or pore structure damage resulting from stress variations.

5. RESULTS AND DISCUSSION

This article refers to the thermal fluid−solid coupling relationship model constructed by scholars such as Zhang[36] in the comprehensive evaluation of the thermal fluid−solid coupling model for high-temperature geothermal extraction. The diffusion−seepage−stress coupling relationship constructed in this study is shown in Figure 6.

The nanopore diffusion field, permeation field, and stress field are interconnected through specific coupling mechanisms, illustrating the dynamic interactions in nanopore gas transport. These fields impact the microscopic behavior of gas including molecular motion, permeability, and pressure distribution. Additionally, they influence the characteristics of the nanopores, such as their structure and fluid dynamics. To evaluate the effectiveness of the microdiffusion−seepage−stress multifield coupling model, a practical case study is used: methane gas diffusion in underground gas storage. Underground gas storage is a key facility for storing natural gas, and the behavior of gas diffusion is crucial to the safety and reliability of gas storage.

Shanxi is one of the major coal producers in China and also one of the provinces rich in CBM resources. The province has about 8.31 trillion cubic meters of coalbed gas resources buried at a shallow depth of 2000 m. By the end of 2020, Shanxi's proven coalbed gas reserves reached 1.06 trillion cubic meters, accounting for 89.83% of the country's total reserves, and its annual gas production was 8.146 billion cubic meters, accounting for 95% of the country's total gas production. In the process of coal mining in Shanxi Province, a large number of gob areas and abandoned mines have been formed that contain valuable coalbed methane resources. According to the data, Shanxi has about 2052 km^2 of potential coal goaf, and it is estimated that there are 72.6 billion cubic meters of residual coal seam gas resources. In this study, an underground gas storage facility is selected in Jincheng, Shanxi Province, which has abundant natural gas production and extensive underground gas storage facilities. The study covered 10 months of simulation time to observe the long-term behavior of gas diffusion.

The boundary conditions are set as follows:

Setting a stable concentration of 11% and a temperature of 293 K is based on typical parameters for underground storage. These parameters are crucial in determining the thermodynamic and fluid dynamic characteristics of the gas in the model, providing an approximate laboratory environment for further simulation of transport phenomena. An inlet pressure of 72 kPa not only simulates typical operating conditions of gas transmission pipelines but also provides the necessary driving force for gas flow. The selection of this parameter is based on the actual operating pressure of on-site gas transmission systems, ensuring the engineering applicability and realism of the model. By simulating different leak rates with diameters of 195.7 and 168.9 mm, the variation in gas diffusion and seepage behavior under different physical conditions is studied. This helps assess the impact of leaks of different scales on gas transmission characteristics, providing a basis for gas leakage risk assessment and control. Setting the outlet pressure to 59.864 and 61.385 kPa reflects the operational pressure of actual gas extraction pipelines. These conditions, based on the pressure range of real working environments, aid in simulating gas transport and distribution under different pressures. The use of nonslip wall conditions is a standard practice for simulating real fluid flow behavior, assuming zero velocity at the gas-wall contact point, accurately describing gas flow characteristics within nanopores, and considering velocity gradients and fluid flow properties.

The Fick's diffusion equation, Darcy's seepage equation, and rock mechanics equation were used as the basis for theoretical

https://doi.org/10.1021/acsomega.4c01572
ACS Omega 2024, 9, 28207−28217

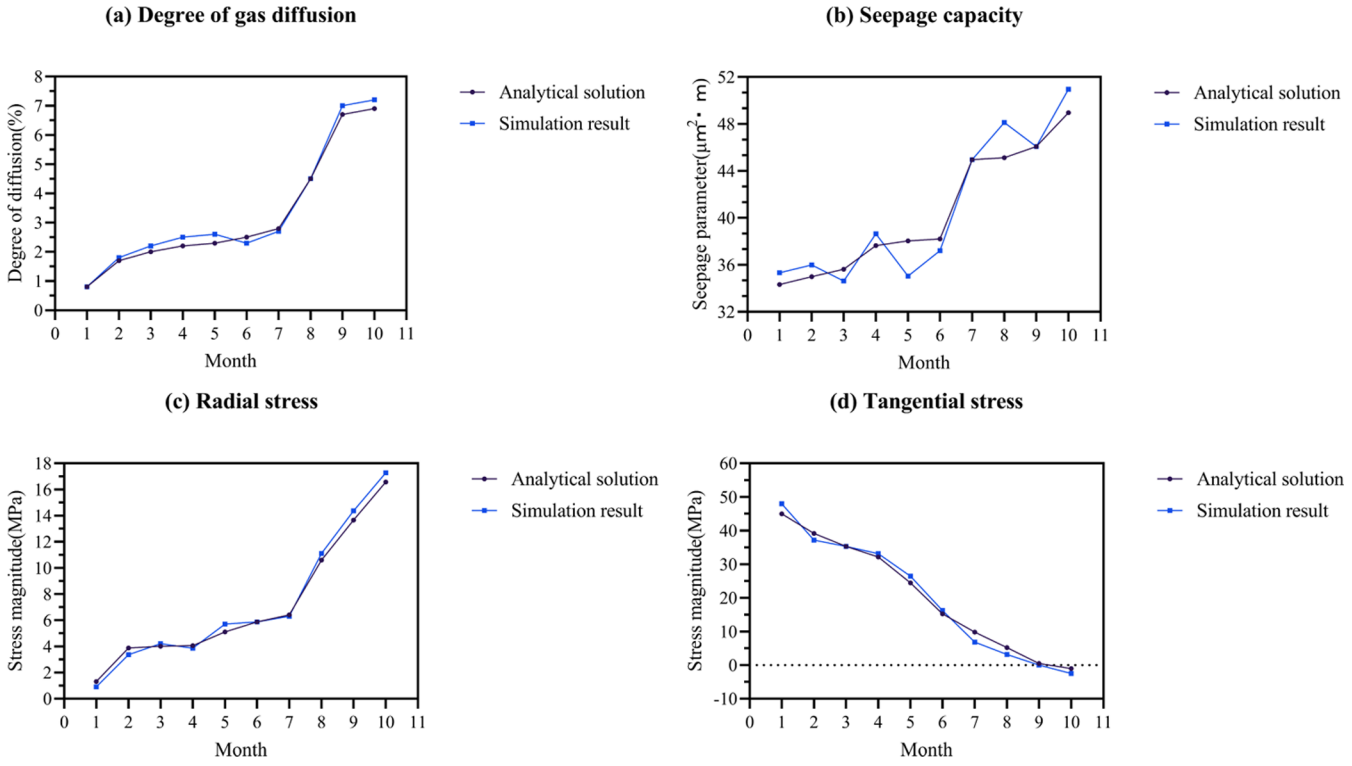

Figure 7. Verification of the multifield coupling model under COMSOL. (a): Gas diffusion degree; (b): permeability; (c): radial stress; and (d): tangential stress.

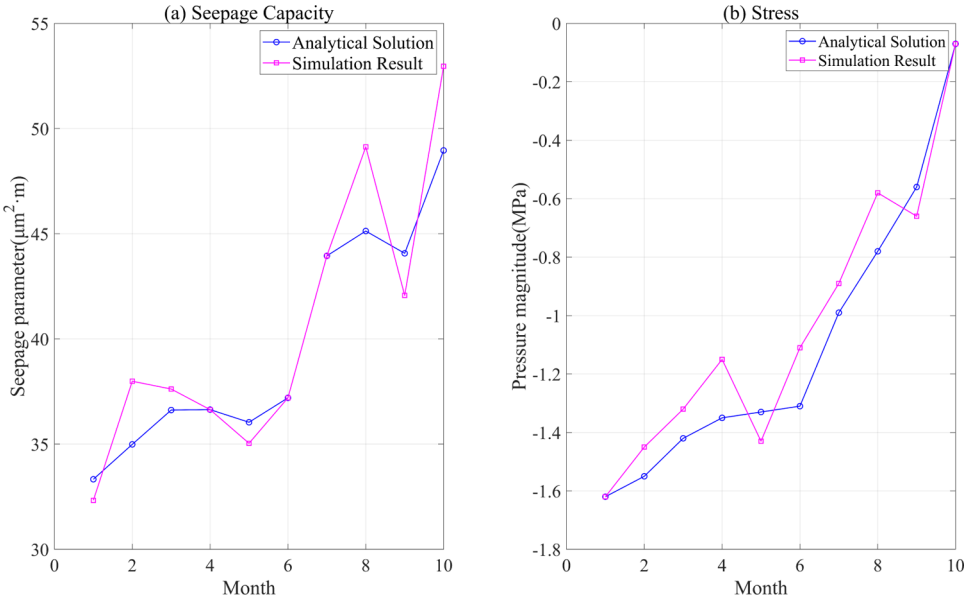

Figure 8. Evaluation of multifield coupling effects of seepage and stress in ANSYS. (a): Seepage capacity and (b): pressure magnitude.

analytical solutions. To verify the accuracy of the model, the simulation findings were compared with known theoretical analytical solutions. Four different numerical simulation tools were used to solve the constructed microdiffusion−seepage−stress multifield coupling model in order to verify the accuracy and reliability of the model.

(1) COMSOL was used to solve the multifield coupling model, considering the interaction of gas diffusion, seepage, and underground stress. The results are shown in Figure 7.

(2) ANSYS software was used for simulation, considering the multifield coupling effect of seepage and stress, as shown in Figure 8.

(3) The open-source CFD (computational fluid dynamics) software OpenFOAM was utilized to establish a multifield coupling model to simulate gas diffusion and seepage.

(4) The CFX solver was used for simulation, considering gas diffusion and seepage. The calculation results under OpenFOAM are shown in Figure 9.

https://doi.org/10.1021/acsomega.4c01572
ACS Omega 2024, 9, 28207−28217

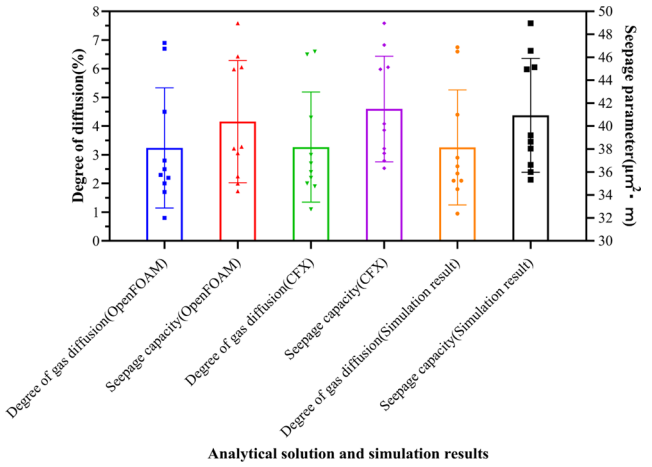

Figure 9. Comparison of the gas diffusion degree and seepage capacity with simulation results under OpenFOAM and CFX.

Figure 7a–d show the calculation results of gas diffusion degree, permeability, radial stress, and tangential stress under COMSOL, respectively. It compared them with the simulation findings of the multifield coupling model constructed in the study. The horizontal axis represents the 10 months tested, while the vertical axis represents the degree of diffusion (%), seepage parameters (μm^2·M), and pressure magnitude (MPa). The data shows that from January to October, the difference between the simulation results and the analytical solutions is very small. In January, both were at 0.8%, while in October, the analytical solution was at 6.9%, and the simulation result was at 7.2%. The slight discrepancy demonstrates the accuracy and reliability of the model in predicting gas diffusion. Regarding permeability, the model also showed a high degree of accuracy. In October, the analytical solution was 48.96 μm^2/m, and the simulation result was 50.96 μm^2/m, indicating the model's sensitivity to permeability. In the simulation of radial stress, the analytical solution in October was 16.57 MPa, and the simulation result was 17.27 MPa, showing that the model accurately reflects the actual stress distribution. In terms of tangential stress, the performance of the model was equally impressive, further confirming its ability to capture subtle changes. The comparison of the data highlights the superiority of the model used in this study, especially in terms of accuracy and reliability in simulating the diffusion, seepage, and stress of nanopore gas.

Figure 8a,b shows the evaluation results of the multifield coupling effect of seepage and stress under ANSYS, which are also compared with the simulation results of the multifield coupling model. The horizontal axis is the month, and the vertical axis is the seepage parameters and pressure magnitude, respectively. The data indicates that from January to October, the difference between the simulation results and the analytical solutions is very small, showing high accuracy of the model in predicting seepage capability. In January, the analytical solution was 33.33 μm^2/m, while the simulation result was 32.33 μm^2/m; in October, the analytical solution was 48.96 μm^2/m, and the simulation result was 52.96 μm^2/m. The results demonstrate that the model can accurately predict seepage behavior under various conditions. In terms of pressure, the model showed sensitivity and high accuracy in capturing subtle changes. The data shows that the simulation results closely followed the analytical solutions throughout the time series, with both being −1.62 MPa in January and −0.07 MPa in October.

Figure 9 visually displays the calculation results of gas diffusion degree and seepage capacity under OpenFOAM, CFX, and multifield coupling models over the 10 months tested. The horizontal axis represents different analytical solutions and simulation results; the left *Y*-axis shows the degree of gas diffusion, and the right *Y*-axis shows the magnitude of the pressure. The data demonstrate that the model shows good consistency and accuracy under different simulation tools. In January, the degree of gas diffusion in OpenFOAM and CFX was 0.8 and 1.1%, respectively, while the multifield coupling model showed a result of 0.95%. In terms of seepage capability, the results from OpenFOAM and CFX were 34.33 and 36.33 μm^2/m, respectively, while the multifield coupling model was 35.33 μm^2/m.

It can be seen that the multifield coupling model constructed by the research institute is close to the actual results in the simulation process of diffusion, seepage, and stress, and the simulation results are well fitted with known theoretical analytical solutions. This indicates that the microdiffusion–seepage–stress multifield coupling model and mathematical methods used by the research institute for nanopore gas have high feasibility in practical applications.

To further determine the model error, the RMSE and MAE between the simulation results and the actual values are calculated, as shown in eqs 19 and 20

$$\mathrm{RMSE} = \sqrt{\frac{\sum_{i=1}^{n} (a_i - \hat{a}_i)^2}{n}} \tag{19}$$

$$\mathrm{MAE} = \frac{\sum_{i=1}^{n} |a_i - \hat{a}_i|}{n} \tag{20}$$

Among them, a_i represents the actual value, and $\hat{a}_i$ represents the simulated value. RMSE is used to measure the overall error between simulated and actual values, while MAE is used to measure the average absolute value between the simulated and actual values. The smaller the values of RMSE and MAE, the higher the prediction accuracy of the model. The results are illustrated in Table 4.

According to Table 4, the constructed multifield coupling model was tested using different tools such as COMSOL,

Table 4. Calculation Outcomes of RMSE and MAE Values for the Multifield Coupling Model

numerical simulation tool	simulated direction	RMSE	MAE
COMSOL	degree of gas diffusion	0.24	0.13
	seepage capacity	0.15	0.17
	radial stress	0.13	0.14
	tangential stress	0.23	0.13
	average	0.19	0.14
ANSYS	seepage capacity	0.24	0.17
	stress	0.14	0.16
	average	0.19	0.17
OpenFOAM	degree of gas diffusion	0.18	0.16
	seepage capacity	0.21	0.16
	average	0.20	0.16
CFX	degree of gas diffusion	0.22	0.16
	seepage capacity	0.18	0.13
	average	0.20	0.15

https://doi.org/10.1021/acsomega.4c01572
ACS Omega 2024, 9, 28207−28217

ANSYS, OpenFOAM, and CFX. The mean values of simulated RMSE for different testing directions were 0.19, 0.19, 0.20, and 0.20, respectively, and the mean values of MAE were 0.14, 0.17, 0.16, and 0.15, respectively. The model can effectively simulate the gas situation in practical applications and accurately evaluate the microdiffusion, seepage, and stress under the degree of nanopores.

6. CONCLUSIONS

This study successfully developed a microdiffusion−seepage−stress multifield coupling model aimed at precisely predicting and managing gas transport behavior in nanopores. This article utilizes molecular dynamics simulation, continuum mechanics, finite element analysis, and porous media modeling. It comprehensively considers the motion trajectory and interaction with the pore walls of gas molecules inside the nanopores. The model was validated by using a case study of methane gas diffusion in underground gas storage. This article used various simulation tools such as COMSOL, ANSYS, OpenFOAM, and CFX. The model exhibits good consistency and accuracy in different testing directions with average RMSE values of 0.19, 0.19, 0.20, and 0.20, respectively. The average MAE values were 0.14, 0.17, 0.16, and 0.15, respectively. In simulations with COMSOL, the RMSE values for gas diffusion, permeability, radial stress, and tangential stress were 0.24, 0.15, 0.13, and 0.23, respectively, and the MAE values were 0.13, 0.17, 0.14, and 0.13, respectively. The results indicated that the model can accurately describe gas transmission within nanopores, exhibiting high predictive accuracy and reliability. It provided crucial theoretical support and practical guidance for the design, optimization, and safe operation of underground gas storage facilities. Meanwhile, when the research model is applied to underground gas storage, it may be influenced by factors such as geological conditions, groundwater levels, and surface activities, and further consideration of the impact of these external factors on the model is needed. To further improve the accuracy and applicability of the model, improvements and refinements can be made in the following aspects. First, by conducting further experimental research to obtain more data on gas under different nanopore structures and conditions, the accuracy of the model can be verified and optimized. Second, more complex numerical calculation methods and simulation tools, such as deep learning techniques and artificial neural networks, can be introduced to better simulate and predict the diffusion, seepage, and stress distribution of gases in nanopores. Finally, by integrating geological exploration and hydrodynamics, among other fields, the model can be further improved to more accurately predict gas transport behavior during underground gas storage processes and to provide more reliable foundations for related engineering design and risk assessment.

AUTHOR INFORMATION

Corresponding Author

Haifeng Wang − *National Engineering Research Center for Coal and Gas Control, China University of Mining and Technology, Xuzhou 221116, China; School of Safety Engineering, China University of Mining and Technology, Xuzhou 221116, China;* orcid.org/0000-0001-7262-7695; Email: 4748@cumt.edu.cn

Authors

Pingdingqi Tuo − *National Engineering Research Center for Coal and Gas Control, China University of Mining and Technology, Xuzhou 221116, China; School of Safety Engineering, China University of Mining and Technology, Xuzhou 221116, China;* orcid.org/0009-0002-9751-3330

Lu Cunyang − *National Engineering Research Center for Coal and Gas Control, China University of Mining and Technology, Xuzhou 221116, China; School of Safety Engineering, China University of Mining and Technology, Xuzhou 221116, China;* orcid.org/0009-0004-4863-4608

Zhang Xinghua − *School of Environment and Safety Engineering, North University of China, Taiyuan, Shanxi 030051, China*

Complete contact information is available at: https://pubs.acs.org/10.1021/acsomega.4c01572

Notes

The authors declare no competing financial interest.

REFERENCES

(1) Sun, J.; Liu, D.; Zhu, X.; Huang, W.; Cheng, L. Experimental investigation on the contribution of gas molecular diffusion to gas mass flux in micro-nano pores. *Geosyst. Eng.* **2020**, *23* (1), 26−36.

(2) Liu, X.; Zhang, L.; Zhao, Y.; He, X.; Wu, J.; Su, S. Shale gas transport in nanopores: Contribution of different transport mechanisms and influencing factors. *Energy Fuels* **2021**, *35* (3), 2033−2047.

(3) Song, W.; Yao, J.; Ma, J.; Sun, H.; Li, Y.; Yang, Y.; et al. Numerical simulation of multiphase flow in nanoporous organic matter with application to coal and gas shale systems. *Water Resour. Res.* **2018**, *54* (2), 1077−1092.

(4) Xu, H.; Yu, H.; Fan, J.; Zhu, Y.; Wang, F.; Wu, H. Two-phase transport characteristic of shale gas and water through hydrophilic and hydrophobic nanopores. *Energy Fuels* **2020**, *34* (4), 4407−4420.

(5) Yu, H.; Xu, H.; Fan, J.; Zhu, Y.-B.; Wang, F.; Wu, H. Transport of shale gas in microporous/nanoporous media: molecular to pore-scale simulations. *Energy Fuels* **2020**, *35* (2), 911−943.

(6) Cychosz, K. A.; Thommes, M. Progress in the physisorption characterization of nanoporous gas storage materials. *Engineering* **2018**, *4* (4), 559−566.

(7) Zhu, Z.; Wang, D.; Tian, Y.; Jiang, L. Ion/molecule transportation in nanopores and nanochannels: From critical principles to diverse functions. *J. Am. Chem. Soc.* **2019**, *141* (22), 8658−8669.

(8) Tesson, S.; Firoozabadi, A. Methane adsorption and self-diffusion in shale kerogen and slit nanopores by molecular simulations. *J. Phys. Chem. C* **2018**, *122* (41), 23528−23542.

(9) Yin, Y.; Qu, Z.; Prodanovic, M.; Landry, C. J. Identifying the dominant transport mechanism in single nanoscale pores and 3D nanoporous media. *Fundam. Res.* **2023**, *3* (3), 409−421.

(10) Gao, Q.; Dong, P.; Liu, C. Study on the influence of shale storage space types on shale gas transport. *ACS Omega* **2021**, *6* (20), 12931−12951.

(11) Yuan, Z.; Misra, R. P.; Rajan, A. G.; Strano, M. S.; Blankschtein, D. Analytical prediction of gas permeation through graphene nanopores of varying sizes: understanding transitions across multiple transport regimes. *ACS Nano* **2019**, *13* (10), 11809−11824.

(12) Yin, Y.; Qu, Z.; Zhu, C.; Zhang, J. Visualizing gas diffusion behaviors in three-dimensional nanoporous media. *Energy Fuels* **2021**, *35* (3), 2075−2086.

(13) Zhang, L.; Liu, C.; Liu, Y.; Li, Q.; Cheng, Q.; Cai, S. Transport property of methane and ethane in K-Illite nanopores of shale: insights from molecular dynamic simulations. *Energy Fuels* **2020**, *34* (2), 1710−1719, DOI: 10.1021/acs.energyfuels.9b04255.

(14) Hu, Z.; Duan, X.; Chang, J.; Zhang, X.; Zhou, S.; Xu, Y.; et al. Multiple Gas Seepage Mechanisms and Production Development Research for Shale Gas Reservoirs from Experimental Techniques and Theoretical Models. *ACS Omega* **2023**, *8* (4), 3571−3585.
(15) Huang, T.; Li, E.; Tao, Z.; Guo, X. A nonlinear seepage model of gas and water transport in multi-scale shale gas reservoirs based on dynamic permeability. *J. Geophys. Eng.* **2018**, *15* (4), 1255−1268.
(16) Wu, S.; Li, Z.; Zhang, C.; Lv, G.; Zhou, P. Nanohydrodynamic Model and Transport Mechanisms of Tight Oil Confined in Nanopores Considering Liquid−Solid Molecular Interaction Effect. *Ind. Eng. Chem. Res.* **2021**, *60* (49), 18154−18165.
(17) Feng, Q.; Xu, S.; Xing, X.; Zhang, W.; Wang, S. Advances and challenges in shale oil development: A critical review. *Adv. Geo-Energy Res.* **2020**, *4* (4), 406−418.
(18) Ohaeri, E.; Eduok, U.; Szpunar, J. Hydrogen related degradation in pipeline steel: A review. *Int. J. Hydrogen Energy* **2018**, *43* (31), 14584−14617.
(19) Li, Y.; Zhao, Q.; Lyu, Q.; Xue, Z.; Cao, X.; Liu, Z. Evaluation technology and practice of continental shale oil development in China. *Pet. Explor. Dev.* **2022**, *49* (5), 1098−1109.
(20) Fan, C.; Yang, L.; Sun, H.; Luo, M.; Zhou, L.; Yang, Z.; et al. Recent Advances and Perspectives of CO2-Enhanced Coalbed Methane: Experimental, Modeling, and Technological Development. *Energy Fuels* **2023**, *37* (5), 3371−3412.
(21) Zhu, W.-Y.; Chen, Z.; Shang, X.-C. Multiphysical field coupling in unconventional oil and gas reservoirs. *Chin. J. Eng.* **2023**, *45* (6), 1045−1056, DOI: 10.13374/j.issn2095-9389.2022.03.29.002.
(22) Chai, D.; Fan, Z.; Li, X. A new unified gas-transport model for gas flow in nanoscale porous media. *SPE J.* **2019**, *24* (02), 698−719.
(23) Ross-Jones, J.; Gaedtke, M.; Sonnick, S.; Radle, M.; Nirschl, H.; Krause, M. J. Conjugate heat transfer through nano scale porous media to optimize vacuum insulation panels with lattice Boltzmann methods. *Comput. Math. Appl.* **2019**, *77* (1), 209−221.
(24) Song, W.; Yin, Y.; Landry, C. J.; Prodanovic, M.; Qu, Z.; Yao, J. A local-effective-viscosity multirelaxation-time lattice Boltzmann pore-network coupling model for gas transport in complex nanoporous media. *SPE J.* **2021**, *26* (01), 461−481, DOI: 10.2118/203841-PA.
(25) Li, Z.; Li, L.; Peng, J.; Karrech, A.; Liu, Y. Model and Experiment of Multiscale Dynamic Permeability in Series for Coalbed Gas Flowing through Micro−Nanopores. *Energy Fuels* **2022**, *36* (18), 10845−10859.
(26) Huang, T.; Cao, L.; Yuan, C.; Chen, P. A novel numerical model of gas transport in multiscale shale gas reservoirs with considering surface diffusion and Langmuir slip conditions. *Energy Sci. Eng.* **2019**, *7* (4), 1315−1332.
(27) Zhang, J.; Pei, G.; Zhang, L. Molecular dynamics simulation of methane gas flow in nanopores. *Petroleum* **2019**, *5* (3), 252−259.
(28) Tian, F.; Liu, Z.; Zhu, W.; Su, W.; Wang, J.; Yang, J.; et al. Experimental Assessment of Combined Contribution of Coal Mass Diffusion and Seepage to Methane Migration under In Situ Stress Conditions. *Energy Fuels* **2023**, *37* (8), 5766−5776, DOI: 10.1021/acs.energyfuels.2c03947.
(29) Sun, J.; Liu, D.; Zhu, X.; Huang, W.; Chen, L. Experimental investigation on shale gas transport characteristics in nanopores under high temperature and high pressure. *Int. J. Oil, Gas Coal Technol.* **2021**, *26* (3), 302−325.
(30) Zhang, X. Shale gas transport model considering gas adsorption and desorption. *Int. J. Energy* **2023**, *2* (2), 51−55.
(31) Sun, Z.; Shi, J.; Wu, K.; Li, X. Gas flow behavior through inorganic nanopores in shale considering confinement effect and moisture content. *Ind. Eng. Chem. Res.* **2018**, *57* (9), 3430−3440.
(32) Jiang, Z.; Wang, W.; Zhu, H.; Yin, Y.; Qu, Z. Review of Shale Gas Transport Prediction: Basic Theory, Numerical Simulation, Application of AI Methods, and Perspectives. *Energy Fuels* **2023**, *37* (4), 2520−2538.
(33) Wang, S.; Shibata, M. S.; Chowdhury, A.; Weber, A. Z. Continuum Modeling of Gas and Ions Transport in a High-Surface-Area Carbon (HSC) Nanopore. *ECS Meet. Abstr.* **2023**, *243* (45), 2486.
(34) Yuan, Z.; Rajan, A. G.; He, G.; Misra, R. P.; Strano, M. S.; Blankschtein, D. Predicting gas separation through graphene nanopore ensembles with realistic pore size distributions. *ACS Nano* **2021**, *15* (1), 1727−1740, DOI: 10.1021/acsnano.0c09420.
(35) Faucher, S.; Aluru, N.; Bazant, M. Z.; Blankschtein, D.; Brozena, A. H.; Cumings, J.; et al. Critical knowledge gaps in mass transport through single-digit nanopores: A review and perspective. *J. Phys. Chem. C* **2019**, *123* (35), 21309−21326, DOI: 10.1021/acs.jpcc.9b02178.
(36) Zhang, W.; Sun, J.; Qu, Z.; Guo, T.; Gong, F.; Zhang, H. Thermal fluid solid coupling model and comprehensive evaluation method for high-temperature geothermal exploitation. *Prog. Geophys.* **2019**, *34* (2), 668−675, DOI: 10.6038/pg2019cc0445.

https://doi.org/10.1021/acsomega.4c01572
ACS Omega 2024, 9, 28207−28217